JOURNAL OF CATALYSIS 141, 583–594 (1993)

Structure and Performance of $LiYO_2$ Methane Coupling Catalysts: Active Phases and Decay Mechanisms

X. ZHANG, D. A. JEFFERSON, AND R. M. LAMBERT[1]

Department of Chemistry, University of Cambridge, Lensfield Road, Cambridge CB2 1EW, United Kingdom

Received August 13, 1992; revised November 24, 1992

X-ray diffraction, high-resolution electron microscopy, and microreactor studies have been used to investigate variations in structure and reactivity of a $LiYO_2$ catalyst during the oxidative coupling of methane. The results indicate that both $LiYO_2$ and small crystallites of Li^+-doped Y_2O_3 are active for methane conversion to ethane and ethylene. An amorphous phase appears during transformation of $LiYO_2$ into Y_2O_3; continued loss of lithium accompanied by formation of larger crystallites of Y_2O_3 gives rise to increased deep oxidation and reduced C_2 production. The deactivation of these catalysts is associated with increase in size and crystallinity of the fluorite-like Y_2O_3 paracrystals, loss of incorporated Li^+, and partial conversion to lithium carbonate. © 1993 Academic Press, Inc.

INTRODUCTION

The oxidative coupling of methane to higher hydrocarbons continues to attract intensive research both in academic and industrial laboratories. Following Keller and Bhasin's original work (*1*), many oxide systems have been found to exhibit promising activity and the subject has been extensively reviewed (*2, 3*). Mixed oxides characterized by the rock salt superstructure constitute a promising class of catalysts, and we have shown that among these, $LiNiO_2$ and $LiYO_2$ are particularly effective (*4, 5*). A comparison between these two systems is interesting for the following reason. Although they possess closely related structures, $LiNiO_2$ is capable of exhibiting redox behavior, whereas $LiYO_2$ is not. Earlier work, including our own, has shown that Ni^{2+}/Ni^{3+} interconversion within the oxide matrix plays a key role in determining the behavior of $LiNiO_2$ as an oxidative coupling catalyst (*4–8*). Since this possibility does not exist in the case of $LiYO_2$, the nature of the catalytically active phase is likely to be quite different.

This paper reports on the performance of $LiYO_2$ catalysts that exhibit very high initial activity and selectivity at ~1000 K. Bulk and surface structural changes in the catalyst are correlated with changes in reactive behavior, permitting an identification of active phases and poisoning mechanisms.

EXPERIMENTAL

$LiYO_2$ was synthesized by solid-state reaction of lithium nitrate and yttrium oxide. The well-mixed reactants were placed in an alumina boat and calcined in air by slowly raising the temperature to 900 K, maintaining this temperature for several hours; this was followed by slow heating to 1100 K, at which temperature the sample was maintained for 15 h. The 500 mg of catalyst that had been pelletized, crushed, and sieved to 500 μm was tested in a 4-mm-i.d. silica tube microreactor at 1000 K at 1 bar total pressure, GHSV of 2250 h^{-1}, with premixed reactant (18% CH_4, 3% O_2, 79% He). Products were analyzed by means of a multiplexed quadrupole mass spectrometer; detailed descriptions of the catalyst preparation and characterization have been given elsewhere (*4, 5*). Powder X-ray dif-

[1] To whom correspondence should be addressed.

0021-9517/93 $5.00
Copyright © 1993 by Academic Press, Inc.
All rights of reproduction in any form reserved.

fraction (XRD) patterns were recorded on a Philips PW1710 horizontal diffractometer using Cu$K\alpha$ radiation. Diffractograms were recorded from $2\theta = 3 - 60°$ with the detector moving in $\Delta 2\theta = 0.025°$ steps to achieve a sufficiently good signal-to-noise ratio for quantitative assessment of structure variations with reaction time.

Catalyst samples taken at different stages of the reaction were deposited from suspension onto copper grids coated with holey carbon films; these were examined by high-resolution electron microscopy (HREM) using a modified JEOL JEM-200CX electron microscope fitted with a special side-entry stage and objective lens (*9*). The objective lens characteristics were Cs = 0.52 mm, Cc = 1.05 mm, giving an interpretable point resolution (*10*) of 1.95 Å and an absolute information limit (measured at 10% of maximum contrast) of 1.75 Å. To preserve structural stability during examination, reduced specimen currents (<0.1 Å cm^{-2}) were employed, and examination was restricted to sub-1000-Å aggregates to ensure maximum heat dissipation from the particles under study.

After correction of objective lens astigmatism and alignment of the objective lens to avoid contrast effects due to inclined illumination (*11*), a series of high-resolution micrographs were recorded from each area of interest at a nominal magnification of ×475,000, with focal increments between successive micrographs of approximately 300 Å. To determine the exact magnification of each series of micrographs, a calibration of true magnification against objective lens focusing voltage was made, using a gold specimen giving 2.04-Å (200) lattice fringes: A further check was made with the specimen of the fresh catalyst where the 4.10-Å (101) lattice fringes of $LiYO_2$ (*12*) could be readily identified and used as an internal calibration. Overall accuracy of magnification was to within 2%. Where the crystallite size was in the sub-100 Å range, phases could be identified only by their lattice spacings, but for larger crystallites, selected area electron diffraction (SAED) patterns were also recorded and used for phase characterization.

RESULTS

Microreactor Studies

Figures 1a and 1b show activity and selectivity variations during methane coupling over a $LiYO_2$ catalyst at 1000 K and GHSV of 2250 h^{-1} as a function of reaction time. The activity (~15% CH_4 conversion) and C_2 selectivity (68%) of the fresh catalyst compare favorably with those reported for other efficient systems (*2*, *3*). Note also that methane conversion increased from ~15 to 25% after 80 min, an effect also observed by Miro *et al.* (*13*) in their studies on $Na/NiTiO_3$ methane coupling catalysts. Significant changes in product selectivity

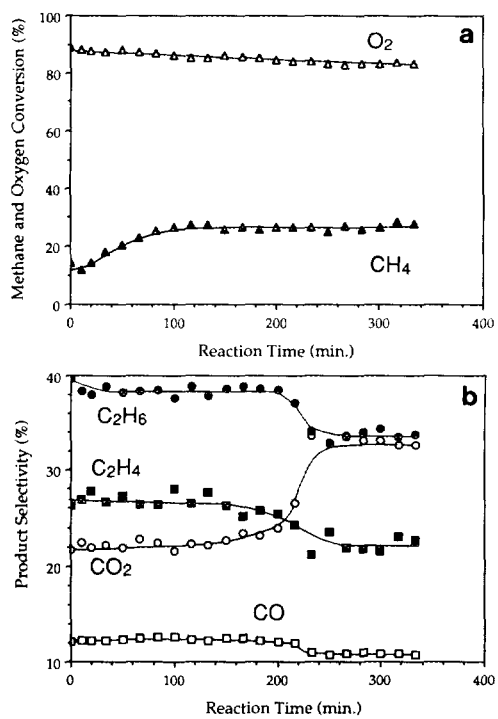

FIG. 1. Reactivity data for methane coupling over $LiYO_2$ at 1000 K and a GHSV of 2250 h^{-1} for ~400 min, (a) methane (▲) and oxygen (△) conversion; analytical error in O_2 detection ~15%, (b) selectivities to ethane (●), ethylene (■), CO (□), and CO_2 (○).

occurred in the interval ~200–240 min. For the first 200 min, selectivities to C_2H_6, C_2H_4, CO, and CO_2 were essentially stable (except for a slight fall in C_2H_6 selectivity) at 38, 26, 12, and 22%, respectively. Beyond this point, C_2 selectivity fell substantially (C_2H_6, 34%; C_2H_4, 21%), while CO_2 production increased substantially from 22 to 33%. Although CO production fell from 12 to 5% during the same interval, overall carbon oxide production was significantly increased.

Because subsequent examination revealed that Y_2O_3 was present in the catalyst under certain conditions, control experiments were carried out on pure Y_2O_3 under conditions identical to those noted above. Methane conversion and C_2 selectivity were 8.0 and 41.2%, respectively, on both counts considerably inferior to the performance of $LiYO_2$.

X-ray Diffraction

XRD measurement (Fig. 2a) confirmed that the fresh $LiYO_2$ catalyst was composed of a single phase of pure $LiYO_2$, no impurity peaks being observed. After ~30 min reaction a new phase that could be confidently identified as Y_2O_3 appeared; diffraction peaks due to Y_2O_3 increased as those due to $LiYO_2$ decreased. Figure 2b shows XRD patterns of the $LiYO_2$ catalyst after 60 min reaction: The peaks labelled α are due to $LiYO_2$, those labelled β being due to Y_2O_3. At this stage, $LiYO_2$ was still the dominant phase. With further reaction, the Y_2O_3 phase became dominant and another new phase (γ) appeared. After ~200 min, there was a marked further decrease in the intensity of $LiYO_2$ reflections and an increase in those due to Y_2O_3. Figure 2c shows the XRD patterns taken after 338 min of reaction; Y_2O_3 is now the dominant phase with $\leq$1% residual $LiYO_2$. The new phase (γ) is most probably Li_2CO_3, although not all the diffraction peaks are in good agreement with literature information and calculations. In particular, we observed a reflection at 49.5° (2θ), while the corresponding calculated value for Li_2CO_3 is 48.7° (2θ). This is discussed below.

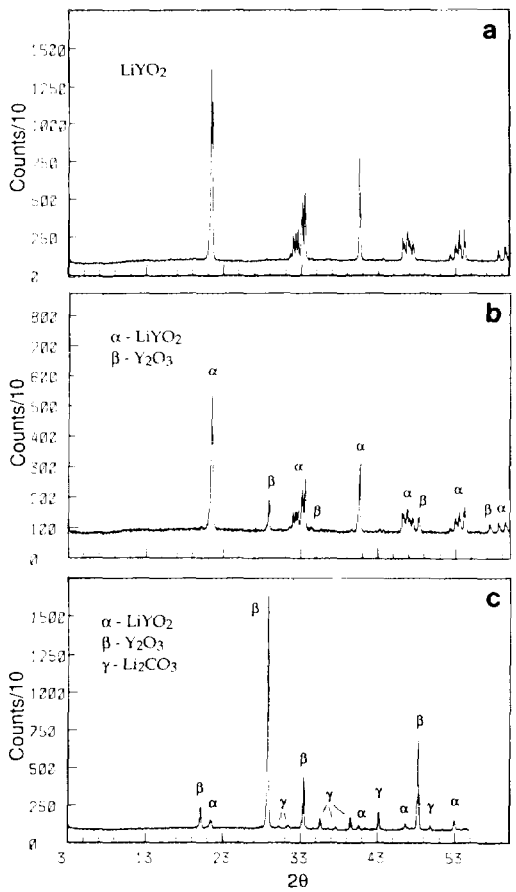

FIG. 2. Powder X-ray diffraction patterns of (a) fresh catalyst, and (b) used catalyst, and (c) deactivated catalyst.

In light of the above findings, control experiments were performed to characterize further the transformation of $LiYO_2$ to Y_2O_3 and Li_2CO_3. Figure 3a shows XRD patterns obtained after calcining a $LiYO_2$ catalyst at 1300 K in air for 60 min. These are similar to those obtained from the used catalyst (Fig. 2b), in which both $LiYO_2$ and Y_2O_3 were observed. Further experiments showed that the extent of $LiYO_2 \rightarrow Y_2O_3$ conversion depended on calcination temperature and time. In the case of the data in Fig. 3a, it is estimated that ~30% Y_2O_3 appeared in the $LiYO_2$ catalyst after calcina-

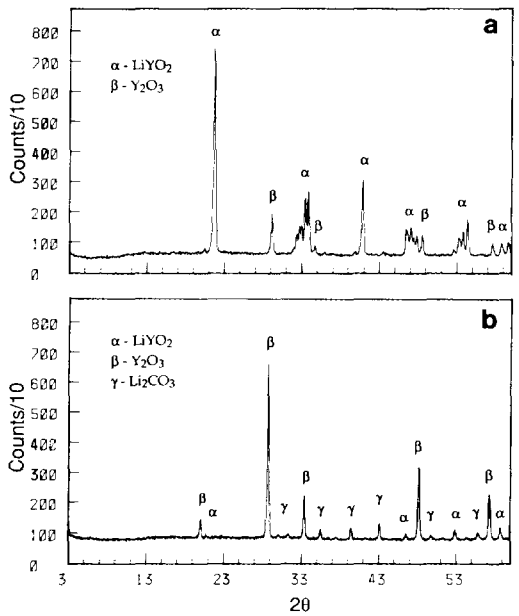

FIG. 3. Powder X-ray diffraction patterns of $LiYO_2$ after (a) recalcination at 1300 K in air for 60 min and (b) heating in CO_2 (10% CO_2/90% He, 30 ml/min) at 1000 K for 60 min.

tion. The interaction of $LiYO_2$ with CO_2 was also examined at 1000 K for 60 min in a flow of 10% CO_2/90% He at ~2250 h^{-1} GHSV. Figure 3b shows XRD patterns resulting from this treatment, and it can be seen that $LiYO_2$ was almost completely converted into Y_2O_3 and Li_2CO_3.

High-Resolution Electron Microscopy

To facilitate discussion of the HREM results, relevant crystallographic data for $LiYO_2$, Y_2O_3, and Li_2CO_3 are summarized in Table 1.

Fresh Catalyst

The HREM specimens comprised clumps of relatively small crystallites (mostly submicrometer) with no pronounced orientational relationship between them; this lack of preferred orientation was confirmed by SAED. Figure 4 shows a typical HREM image of the fresh catalyst. The general surface morphology was that of a smooth, relatively clean surface (no carbon contamination was visible) with no distinct features. Although lattice fringes extended right up to the actual surface, there was a distinct absence of any surface features such as steps: All such discontinuities were "rounded-over." This type of surface is typical of material prepared by solid-state synthesis at relatively low temperature (*16*).

As noted above, the nominal magnification of all the micrographs is 5.463×10^6. However, determination of an exact value comes from consideration of lattice spacings in the phases that might be present. Assuming that Li_2CO_3 is completely absent in the fresh catalyst, the largest spacing should correspond to the {101} fringes in $LiYO_2$. This is shown clearly in Fig. 4: Taking these as 4.100 Å gives a true magnification of 5.247×10^6; all quoted d-spacings are obtained on this basis.

In addition to the typical structure shown in Fig. 4, a few crystals of the type shown in

TABLE 1

Crystal Structure Parameters of Relevant Phases

Phase	Structure	Parameters	d-spacings (Å)[a]	Ref.
$LiYO_2$	Tetragonal	a = 4.44 Å c = 10.69 Å	$d_{(101)}$ = 4.100, $d_{(103)}$ = 2.779 $d_{(004)}$ = 2.673, $d_{(200)}$ = 2.220	(*12*)
Y_2O_3	Cubic	a = 10.605 Å	$d_{(222)}$ = 3.061, $d_{(400)}$ = 2.651 $d_{(440)}$ = 1.875	(*14*)
Li_2CO_3	Monoclinic	a = 8.39 Å, b = 5.00 Å c = 6.21 Å, β = 114.5°	$d_{(110)}$ = 4.18, $d_{(200)}$ = 3.82	(*15*)

[a] Calculated values of largest d-spacings.

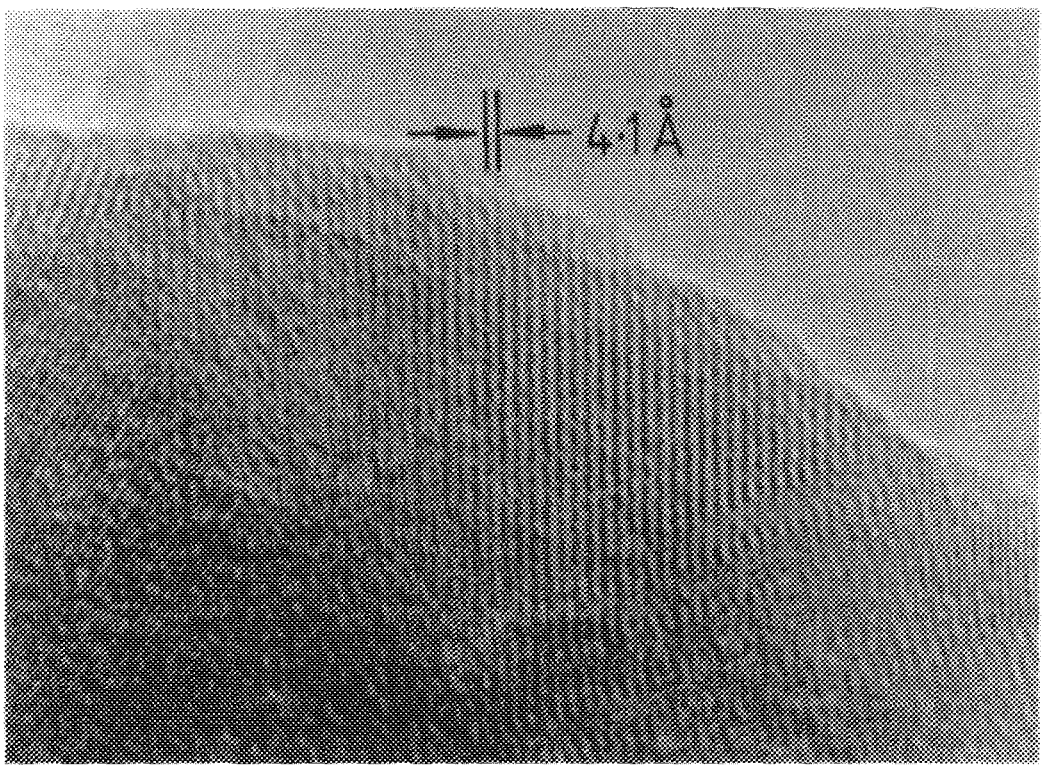

FIG. 4. Typical HREM images of the fresh $LiYO_2$ catalyst, showing the 4.1 Å spacing characteristic of $LiYO_2$.

Fig. 5 were also observed; in this case there is definite evidence of surface steps. Such crystals were relatively large (although still <1 μm) and exhibited lattice fringes inclined to the edge that extended into the bulk of the specimen. *d*-spacings of three such sets of fringes were 3.145, 3.145, and 2.573 Å; the angles between them were 55.5°.

Used Catalyst

At magnifications below $\times 100{,}000$, the used catalyst appeared very similar to the fresh sample, having the same degree of aggregation and the same overall surface appearance. At higher magnifications, however, most crystals exhibited considerable differences in surface structure. Typical examples are shown in Figs. 6 and 7, which are taken from different areas on the same specimen aggregate. In Fig. 6a, areas showing 4.100-Å fringes are still readily apparent (A), indicating that $LiYO_2$ was still present, although these fringes were less common than in the fresh sample and rarely extended to the crystal edges. In addition, the Y_2O_3-like areas (B) were much more common.

The most significant differences are apparent at the specimen edges, where small crystallites have developed, as exemplified by the surface protuberance in Fig. 6b. Here a small paracrystal ~40 Å across is shown: The fringe spacing (3.1 Å) is compatible with fluorite-like Y_2O_3 in [110] projection, and the overall contrast is very similar to that normally observed in CeO_2, another fluorite-like oxide (*17*). Also of interest is an apparently amorphous surface phase, shown in Fig. 7. This observation,

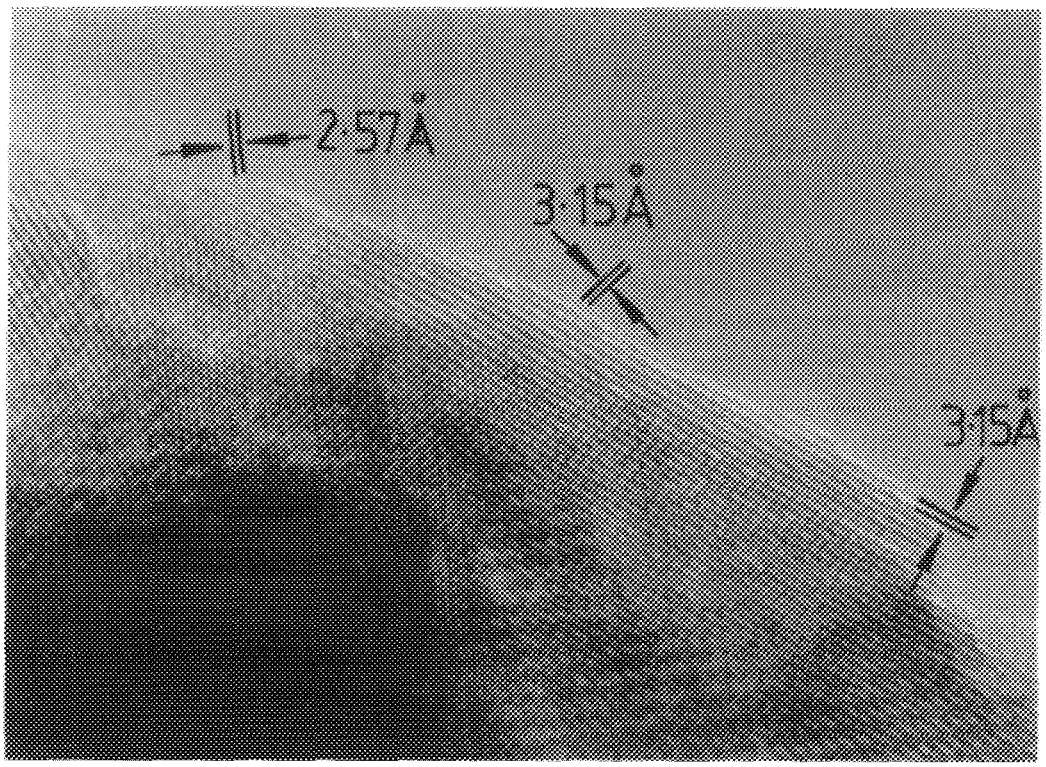

FIG. 5. HREM images of the fresh catalyst showing three sets of fringes (spacings 3.145, 3.145, and 2.573 Å) corresponding closely to those of the Y_2O_3 structure.

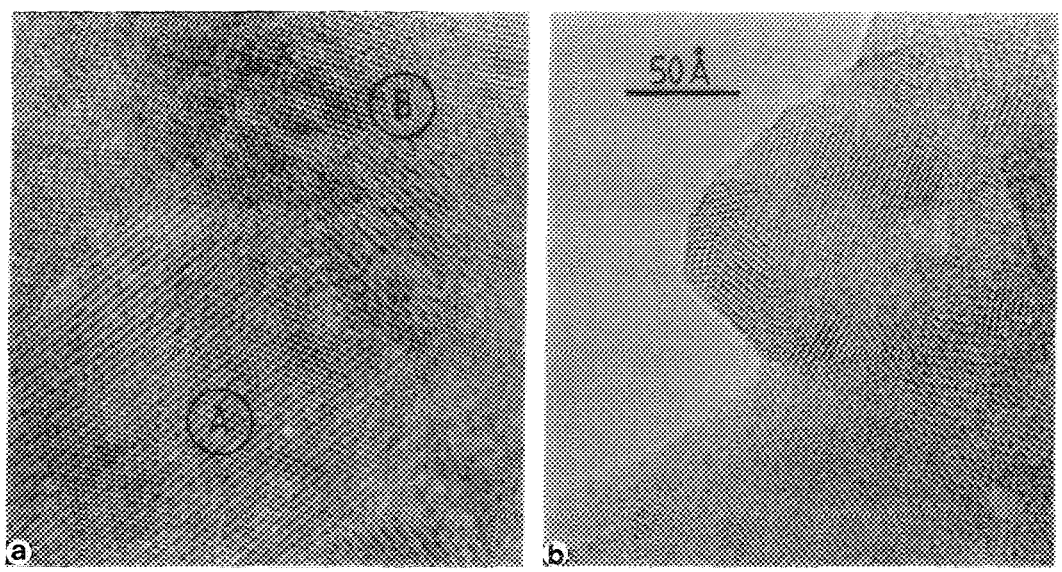

FIG. 6. (a) HREM images of the used catalyst, showing some regions (A) with a 4.1-Å spacing and adjacent areas with 3.1-Å fringes (B). (b) The margin of the same crystal, showing development of micrographs with 3.1-Å spacings.

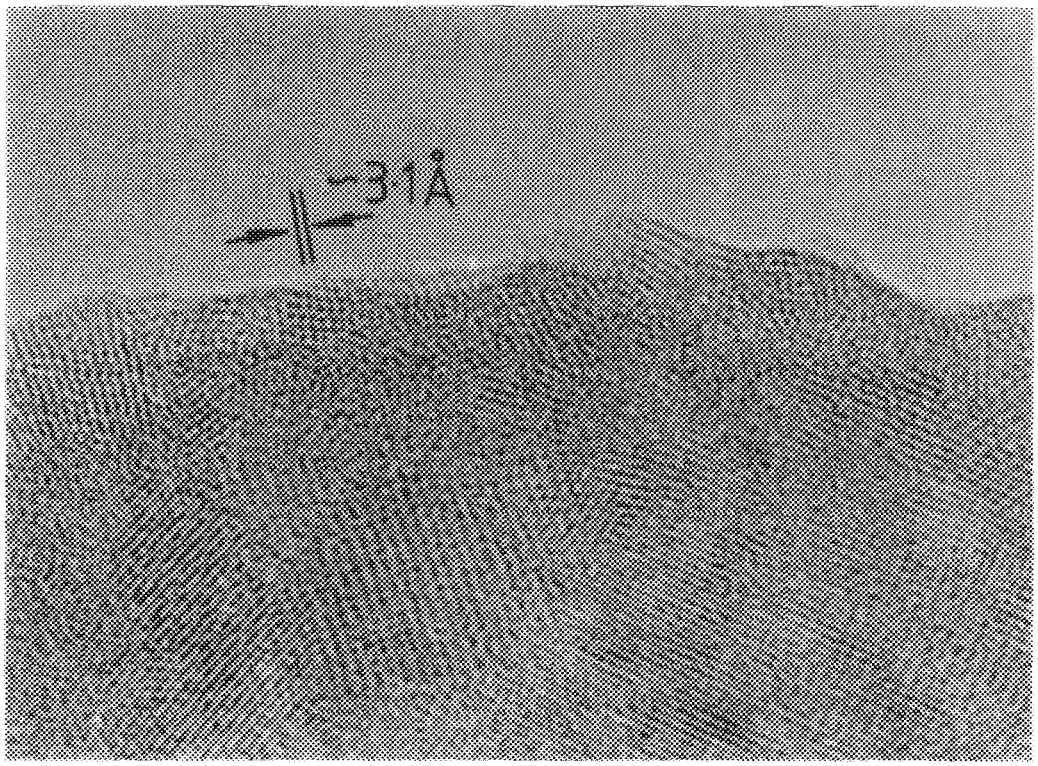

FIG. 7. HREM images of the used catalyst taken from different areas on the same specimen aggregate as Fig. 6, showing an amorphous phase coupled with regions showing fringes of approximately 3.1-Å spacing.

coupled with the presence of similar closely spaced fringes (Fig. 6), suggests that the paracrystals develop from the parent material by transformation of an amorphous intermediate.

Deactivated Catalyst

The deactivated catalyst differed substantially from both the fresh and used materials. The specimen clearly consisted of two phases: (i) large, approximately hexagonal-shaped crystals, which gave clear SAED patterns and had not been observed previously, and (ii) much smaller crystallites, which occurred either in large, micrometer-sized clusters or attached to the margins of the crystals of the first phase. A representative micrograph of the large crystals is shown in Fig. 8. In addition to the 3.1-Å fringes due to the small crystal identified as Y_2O_3, there are 4.28- and 7.52-Å fringes due to the large crystal. The smaller crystallites shown in Fig. 9 are characterized by 3.1-Å fringe spacings with relative inclination of 55.5°. SAED patterns from the large crystals were obtained in two orientations that correspond to low-index axes of projection. Figure 10 shows one of the patterns giving an axial ratio of 1.0 and an interaxial angle of 60°.

DISCUSSION

Fresh Catalyst: Activation and Steady-State Performance

$LiYO_2$ has an ordered rock salt superstructure consisting of mixed cation layers between layers of closest-packed O^{2-} (*18*). The XRD data (Fig. 2a) indicate that the fresh catalyst is a single phase consisting of this material. It gives rise to very high se-

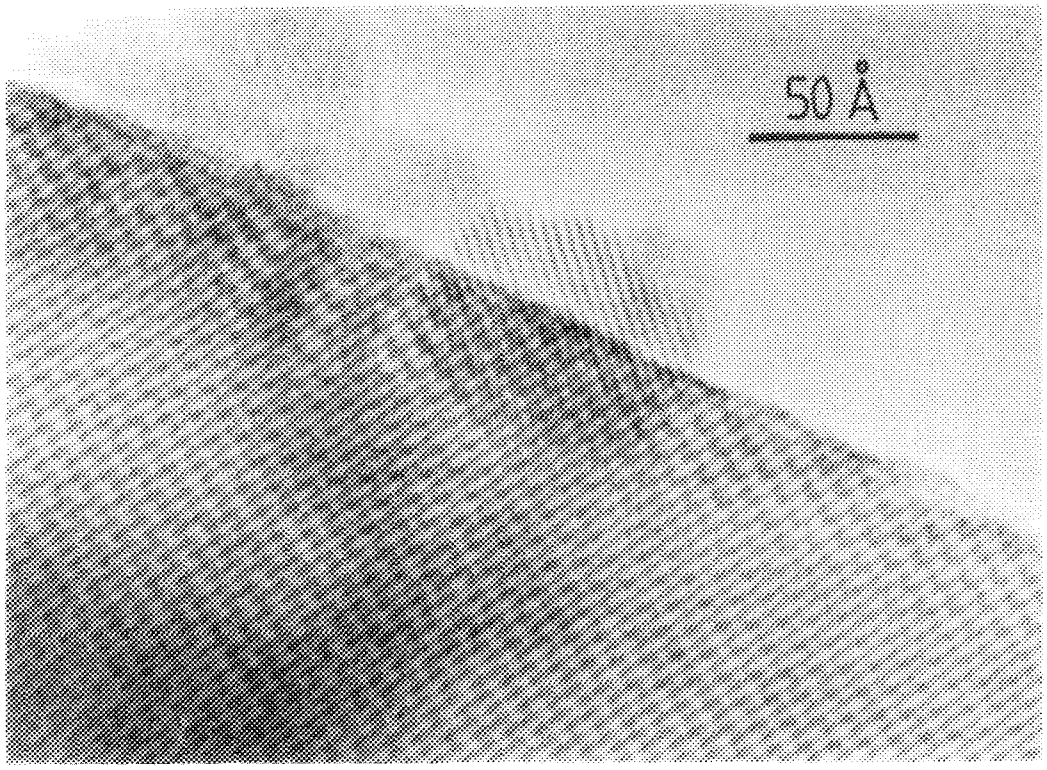

FIG. 8. HREM images of the deactivated catalyst showing large crystals with small crystals attached.

lectivities toward C_2 formation, although initial methane conversion is about 40% lower than that characteristic of the used catalyst (Fig. 1). These results suggest that $LiYO_2$ is an active phase for methane oxidative coupling. This inference is confirmed by the HREM results, which clearly indicate that $LiYO_2$ is the principal phase in the fresh catalyst, even on the microcrystalline scale. The minority phase (Fig. 5) appears to be a cubic structure, the observed fringes arising from the {222} and {400} planes of Y_2O_3. However, the observed lattice spacings are significantly different ($\sim \pm 0.1$ Å) from those characteristic of pure Y_2O_3, suggesting that some Li^+ may be incorporated into the Y_2O_3. This minority phase was invisible to XRD, suggesting that it comprised $<1\%$ of the fresh catalyst.

The reaction data (Fig. 1) show that selectivity varied relatively little over the first 200 min, although there was a significant increase in methane conversion. Taken together, these two observations imply the formation of a carbon-containing product that does not appear in the gas phase. Carbonate formation on the catalyst seems the most likely explanation, and indeed Li_2CO_3 is detected at sufficiently long reaction times (see below). During this same interval, XRD measurements show the appearance of a new phase (Y_2O_3) whose amount increases with time while the amount of $LiYO_2$ decreases. This is an interesting observation, given the relatively stable (good) performance of the catalyst and the fact that pure Y_2O_3 itself is known to be only a modest catalyst. It therefore appears that the Y_2O_3 produced by decomposition of $LiYO_2$ must differ in some significant way

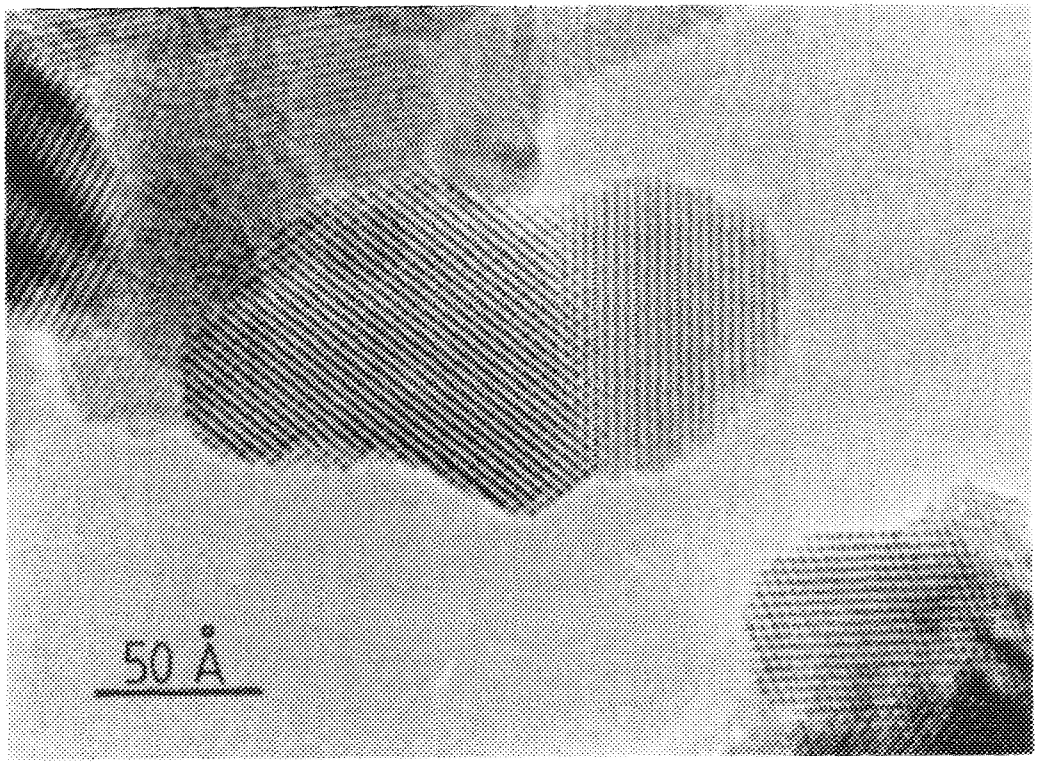

FIG. 9. HREM images of the deactivated catalyst showing small crystals of 3.1-Å fringe spacing with some surface steps visible.

from pure Y_2O_3. Here, the HREM measurements provide the crucial evidence. They reveal the presence of small paracrystals of a fluorite-like Y_2O_3 structure (Fig. 6) whose measured fringe spacings indicate the incorporation of Li^+ into the oxide structure. Related to this is the observation of an amorphous phase (Fig. 7): The production of such a phase seems highly likely during the transformation of $LiYO_2$ to Y_2O_3. The nature of the oxygen sublattice changes from fcc in the former to simple cubic in the latter, and in addition a large number of ordered oxygen vacancies must be generated, involving considerable disruption of the anion lattice during interconversion of the two phases amounting to a complete recrystallization. The implication is that the stable, active, and selective catalyst consists of a mixture of $LiYO_2$ and paracrystalline Li^+-doped Y_2O_3 almost certainly by reducing the number of oxygen vacancies required. It seems likely that lithium incorporation stabilizes the small crystallites of Y_2O_3. It is also possible that the amorphous phase (present in significant amounts) plays some role in the reaction. Where this amorphous region breaks out at the surface (see Fig. 7), one might expect extremely active sites to be generated; such exceptionally active sites might also be present at the stepped surfaces present on the Li^+-doped Y_2O_3 paracrystals.

The increase in methane conversion that occurs over the first ~80 min indicates that some change must be occurring in the catalyst. Miro *et al.* (*13*) have observed similar behavior in the case of $Na/NiTiO_3$ catalysts. This increase may be associated with an increase in catalyst surface area that oc-

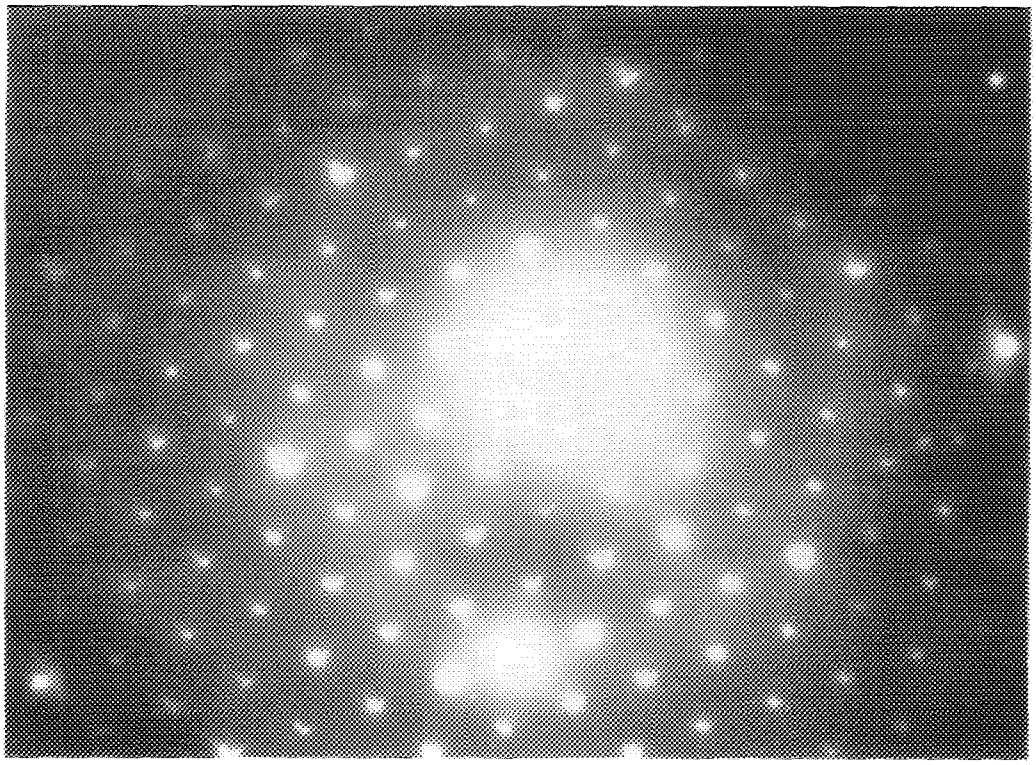

FIG. 10. SAED patterns from the large crystals. Axial ratio = 1.0 and interaxial angle = 60°.

curs during $LiYO_2 \rightarrow Y_2O_3$ (Li) interconversion. It may also reflect the production of sites of high specific activity (*2*) and/or sacrificial consumption of lattice oxygen from the Y_2O_3 phase (*18*).

Catalyst Deactivation

Figure 1 shows that a very marked decline in catalyst performance occurs after ~200 min; C_2 selectivity falls to 55% while CO_2 selectivity rises to 33%, carbon balance being maintained within the experimental error (±5%) in the period following ~200 min reaction, implying that the increase in CO_2 production observed during this stage is not associated with decomposition of Li_2CO_3. These observations, and the simultaneous fall in CO production at constant methane conversion, are consistent with an increase in the number of deep oxidation sites on the catalyst. The fact that the loss in selectivity that occurs at ~200 min is not accompanied by detectable changes in reactant conversion deserves comment. Given the constant level of CH_4 conversion, one might expect some increase in O_2 conversion at ~240 min associated with the increased CO_2 production. Our analytical error for oxygen is ~15% and may have obscured any such effect. More significantly perhaps, the XRD and HREM measurements show that the Y_2O_3(Li) $\rightarrow Y_2O_3$ transformation is well advanced by ≳200 min. The onset of sacrificial consumption of lattice oxygen from Y_2O_3 at this point could then account for the increase in CO_2. A quantitative valuation of the limiting "worst" case, i.e., all additional oxygen required in the interval 240–340 min comes from Y_2O_3, indicates that at the end of the experiment the stoichiometry of the latter would be $Y_2O_{2.983}$,

which is well within the known limits of reduction of Y_2O_3 (*18*). The XRD data show that the $LiYO_2 : Y_2O_3$ ratio in the deactivated catalyst had fallen to 0.05 : 1.0 after 338 min. A significant amount of Li_2CO_3 was also present at this point. Note that not all the diffraction peaks due to Li_2CO_3 are consistent with those of the pure substance, suggesting that yttrium incorporation may have occurred (see below). Interestingly, the performance of this deactivated, largely Y_2O_3(Li)-containing catalyst, both in terms of methane conversion and C_2 selectively is still superior to that of pure Y_2O_3 (*4*).

The HREM data show that the deactivated catalyst consists of two phases with very different crystallite sizes. The smaller crystallites (Fig. 9) may be identified as Li-doped Y_2O_3 from their {222} and {440} lattice spacings. The average particle diameter was ~100 Å, and the overall state of crystallinity was comparable to that of bulk material—*much higher than in the paracrystalline particles of Y_2O_3(Li) characteristic of the active and selective phase*. No trace of the quasi-amorphous phase was found. SAED patterns obtained from particles of the second phase (Fig. 10) are similar in some respects to those expected from Li_2CO_3. However, a detailed calculation of reciprocal lattice spacings shows that these are not compatible with pure Li_2CO_3, even when allowance is made for calibration errors due to the strong objective lens. For example, in Fig. 8, the reciprocal lattice spacing should correspond to those of the {110} and {200} planes of Li_2CO_3 (4.18 and 3.82 Å, respectively); the observed values are ~4.28 and 7.52 Å. Discrepancies are also apparent in the direct space image. The large pseudo-hexagonal crystal giving rise to the SAED pattern (Fig. 10) carries fluorite-like particles on its surface. Some of the lattice spacings of the large crystal are significantly greater than those characteristic of pure Li_2CO_3. Thus the fringes in this crystal yield spacings of 4.28 and 7.52 Å; the former is compatible with pure Li_2CO_3 but the latter is certainly not—nor is the interplanar angle of 90°. These results can only be reconciled with the accepted structure of Li_2CO_3 in terms of the formation of a $(\sqrt{3} \times \sqrt{3})R30°$ superlattice in the x–y plane, which would account for both the observed fringe spacings and the SAED patterns. How might such a superlattice arise? An obvious possibility is that it is caused by incorporation of yttrium into the Li_2CO_3. Such an interpretation would be compatible with the relative proportions of the two phases (large crystals of Li_2CO_3 and small Y_2O_3(Li) particles): There are not enough of the latter to account for all the yttrium in the specimen, suggesting that some of this yttrium must go into the Li_2CO_3 majority phase. Recall that the XRD data (γ peaks in Fig. 2b) are not in good agreement with calculated values based on pure Li_2CO_3, which lends strong support to this view.

It seems clear that lithium, either in the mixed oxide $LiYO_2$ or incorporated in Y_2O_3, is an essential ingredient for an active and selective catalyst. Reaction products can act to degrade catalytic performance by accelerating the loss of lithium from these active phases. Thus we have shown that Li is removed from the catalyst at high temperatures, possibly as Li_2O or, in the presence of H_2O, even more readily as LiOH (*19, 20*). CO_2 exacerbates these effects by inducing the transformation of $LiYO_2$ to Li_2CO_3.

CONCLUSIONS

1. $LiYO_2$ is an active and selective methane coupling catalyst. Under reaction conditions it undergoes decomposition to Y_2O_3.

2. This reactively produced Y_2O_3 is generated in a paracrystalline form and incorporates lithium. It seems likely that the $LiYO_2 \rightarrow Y_2O_3$(Li) transformation proceeds via an amorphous phase.

3. Catalyst deactivation is associated with loss of Li from the oxide phases, increase in size and crystallinity of the Y_2O_3(Li), and Li_2CO_3 formation. It seems

likely that the catalytically efficient Y_2O_3(Li) paracrystals are stabilized by their lithium content.

REFERENCES

1. Keller, G. E., and Bhasin, M. M., *J. Catal.* **73,** 9 (1982).
2. Lee, J. S., and Oyama, S. T., *Catal. Rev. Sci. Technol.* **28,** 249 (1988).
3. Hutchings, G. J., Woodhouse, J. R., and Scurrell, M. S., *Chem. Soc. Rev.* **18,** 251 (1989).
4. Ungar, R. K., Zhang, X., and Lambert, R. M., *Appl. Catal.* **42,** L1 (1988).
5. Zhang, X., Ph.D. thesis, University of Cambridge, 1990.
6. Moggridge, G. D., Badyal, J. S. P., and Lambert, R. M., *J. Catal.* **132,** 92 (1991).
7. Otsuka, K., Liu, Q., Hatano, M., and Morikawa, A., *Inorg. Chim. Acta.* **118,** L24 (1986).
8. Hatano, M., and Otsuka, K., *J. Chem. Soc. Faraday Trans. 1* **85,** 199 (1989).
9. Jefferson, D. A., Thomas, J. M., Millward, G. R., Tsuno, K., Harriman, A., and Brydson, R. D., *Nature* **323,** 428 (1986).
10. Cowley, J. M., *Chem. Scr.* **79,** 279 (1979).
11. Smith, D. J., Saxton, W. O., O'Keefe, M. A., Wood, R. J., and Stobbs, W. M., *Ultramicroscopy* **11,** 263 (1983).
12. Hoppe, W., *Angew. Chem.* **71,** 457 (1959).
13. Micro, E. E., Santamaria, J. M., and Wolf, E. E., *J. Catal.* **124,** 467 (1990).
14. Donnay, J. D. H., and Donnay, G., "Crystal Data Tables," American Crystallographic Association, Washington, D. C., 1963.
15. Zemann, J., *Acta Crystallogr.* **10,** 664 (1957).
16. Legrouri, A., Baird, T., and Fryer, J. R., *Inst. Phys. Conf. Ser.* **93,** 289 (1988).
17. Cochrane, H. D., Hutchison, J. L., and White, D., *Ultramicroscopy* **31,** 138 (1989).
18. Clark, G. M., "The Structures of Non-Molecular Solids," Applied Scientific, London, 1972.
19. Bach, R. O., "Lithium, Current Applications in Science, Medicine, and Technology," Wiley, New York, 1985.
20. Ostroushko, Yu. I., *et al.*, "Lithium, its Chemistry and Technology," p. 60. Trans. H. Basil, Office of Technical Services, U.S. Dept. of Commerce, Washington, 1962.